Journal of Cerebral Blood Flow & Metabolism (2015) 35, 1005–1014

www.jcbfm.com

ORIGINAL ARTICLE

Gliovascular disruption and cognitive deficits in a mouse model with features of small vessel disease

Philip R Holland[1,8], James L Searcy[2], Natalia Salvadores[2], Gillian Scullion[2], Guiquan Chen[2], Greig Lawson[2], Fiona Scott[2], Mark E Bastin[3], Masafumi Ihara[4], Rajesh Kalaria[5], Emma R Wood[6], Colin Smith[7], Joanna M Wardlaw[3] and Karen Horsburgh[1]

Cerebral small vessel disease (SVD) is a major cause of age-related cognitive impairment and dementia. The pathophysiology of SVD is not well understood and is hampered by a limited range of relevant animal models. Here, we describe gliovascular alterations and cognitive deficits in a mouse model of sustained cerebral hypoperfusion with features of SVD (microinfarcts, hemorrhage, white matter disruption) induced by bilateral common carotid stenosis. Multiple features of SVD were determined on T2-weighted and diffusion-tensor magnetic resonance imaging scans and confirmed by pathologic assessment. These features, which were absent in sham controls, included multiple T2-hyperintense infarcts and T2-hypointense hemosiderin-like regions in subcortical nuclei plus increased cerebral atrophy compared with controls. Fractional anisotropy was also significantly reduced in several white matter structures including the corpus callosum. Investigation of gliovascular changes revealed a marked increase in microvessel diameter, vascular wall disruption, fibrinoid necrosis, hemorrhage, and blood–brain barrier alterations. Widespread reactive gliosis, including displacement of the astrocytic water channel, aquaporin 4, was observed. Hypoperfused mice also demonstrated deficits in spatial working and reference memory tasks. Overall, gliovascular disruption is a prominent feature of this mouse, which could provide a useful model for early-phase testing of potential SVD treatment strategies.

Journal of Cerebral Blood Flow & Metabolism (2015) **35,** 1005–1014; doi:10.1038/jcbfm.2015.12; published online 11 February 2015

Keywords: cognition; diffusion-tensor imaging; hypoperfusion; magnetic resonance imaging; small vessel disease

INTRODUCTION

Cerebral small vessel disease (SVD) is a major cause of age-related cognitive decline and dementia.[1] Hypertension is proposed to be a common risk factor (although it explains only a small proportion of imaging-determined SVD) and cerebral amyloid angiopathy is commonly present on pathologic examination.[2,3] Clinically, SVD is associated with early impairment of attention and executive function with slowing of information processing and motor deficits.[1] These clinical manifestations result primarily from the occurrence of lesions in the cerebral white matter, multiple lacunes within subcortical structures, atrophy, and, in some cases, microbleeds in deep gray matter, white matter, or at the corticosubcortical junction, identified by neuroimaging.[2,4] White matter lesions, associated with increased extracellular fluid, varying degrees of myelin and axonal pathology, and glial responses, are predominantly detected as hyperintense regions on fluid attenuation inversion recovery and T2-weighted magnetic resonance imaging (MRI).[5] Lacunes, which present as hypointense regions on fluid attenuation inversion recovery or T1-weighted MRI or hyperintense on T2-weighted MRI, are small deep cavities thought to result from small infarcts, which commonly occur in subcortical areas including the white matter and basal ganglia.[6] Cerebral microbleeds are seen as small hypointense dots on T2*- or susceptibility-weighted MRI and are thought to correspond with perivascular hemorrhages.[7] The pathologic correlates of these radiologic features include extensive vascular disruption associated with fibrinoid necrosis, arteriosclerosis, and collagen deposition.[8] Endothelial failure with altered blood–brain barrier (BBB) permeability is postulated as one pathogenetic component underlying the pathophysiology of SVD.[9] The integrity of the BBB critically depends on the cross-talk between endothelial cells, pericytes, astrocytes, and endfeet processes, which closely contact microvessels comprising the gliovascular unit.[10] Damage to selective components of the gliovascular unit may additionally contribute to the pathophysiology of SVD.

Currently available animal models mimic selective aspects of SVD (for reviews see Hachinski *et al*[11] and Bailey *et al*[12]). One model, the spontaneously hypertensive stroke prone rat develops arteriolar wall thickening, subcortical lesions, enlarged perivascular spaces, and cortical infarcts and hemorrhages, which are

[1]Centre for Neuroregeneration, Centre for Cognitive Ageing and Cognitive Epidemiology, University of Edinburgh, Edinburgh, UK; [2]Centre for Neuroregeneration, University of Edinburgh, Edinburgh, UK; [3]Centre for Cognitive Ageing and Cognitive Epidemiology, Scottish Imaging Network, A Platform for Scientific Collaboration (SINAPSE), Centre for Clinical Brain Sciences, University of Edinburgh, Edinburgh, UK; [4]Department of Stroke and Cerebrovascular Diseases, National Cerebral and Cardiovascular Center Hospital, Osaka, Japan; [5]Institute of Neuroscience, Newcastle University, Campus for Ageing and Vitality, Newcastle upon Tyne, UK; [6]Centre for Cognitive and Neural Systems and Centre for Cognitive Ageing and Cognitive Epidemiology, University of Edinburgh, Edinburgh, UK and [7]Centre for Clinical Brain Sciences, University of Edinburgh, Edinburgh, UK. Correspondence: Professor K Horsburgh, Centre for Neuroregeneration, Centre for Cognitive Ageing and Cognitive Epidemiology, University of Edinburgh, Chancellor's Building, 49 Little France Crescent, Edinburgh EH16 4SB, UK.
E-mail: karen.horsburgh@ed.ac.uk
[8]Current Address: Department of Basic and Clinical Neuroscience, Institute of Psychiatry, Psychology and Neuroscience, King's College London, London, UK.
This work was supported by grants from Help the Aged/Age UK (Disconnected Mind programme), the Alzheimer Society, Alzheimer Research UK, AXA Research Fund, and The University of Edinburgh Centre for Cognitive Aging and Cognitive Epidemiology, part of the cross council Lifelong Health and Wellbeing Initiative (G0700704/84698). The Scottish Funding Council and the British Heart Foundation provided the MRI scanner (BHF CI/05/004).
Received 29 October 2014; revised 12 January 2015; accepted 13 January 2015; published online 11 February 2015

exacerbated with hypertension.[12–15] Blood–brain barrier breakdown, evident by the leakage of immunoglobulin G and dextran, as well as the aggregation of platelets in the vicinity of vascular stases has also been observed.[16,17] Furthermore, ultrastructural changes to astrocytic endfeet in the spontaneously hypertensive stroke prone rat model are indicative of changes in the gliovasculature.[18] Models of chronic cerebral hypoperfusion reproduce diffuse white matter damage and behavioral impairments relevant to SVD.[19–24] A murine hypoperfusion model of bilateral carotid artery stenosis using microcoils[19–22] has been instrumental in exploring early molecular events in white matter at a time when there is an impairment in working memory in the absence of other behavioural changes.[20] One study has described hippocampal hypometabolism and atrophy with sustained hypoperfusion,[24] but the longer-term pathologic, including gliovascular alterations, and radiologic consequences of hypoperfusion have not yet been fully investigated.

Although there is no association between carotid stenosis and SVD in humans,[25] small vessel changes have been linked to histologic features that have been interpreted as representing local hypoperfusion of as yet unknown cause.[26] We therefore hypothesized that sustained hypoperfusion would produce progressive pathologic and cognitive features similar to those seen in SVD. Our study shows that, in response to sustained cerebral hypoperfusion over 6 months in mice, the model develops certain key features of SVD: namely small subcortical ischemic lesions and hemorrhages, cerebral atrophy and white matter changes, and memory impairments. Furthermore, these features were coincident with prominent disruption of the gliovasculature including the BBB, which may be potential therapeutic targets in SVD.

MATERIALS AND METHODS

Animals

Male C57Bl/6J mice ($N = 142$; for details see Supplementary Information and Supplementary Table 1) weighing 25 to 30 g underwent chronic cerebral hypoperfusion[20] via bilateral common carotid artery stenosis using microcoils (coil internal diameter of 0.18 mm) or a sham procedure and recovered for 1 or 6 months. At the outset, mice were coded and randomly assigned to experimental groups for MRI, behavioral, pathologic, and biochemical investigations. Investigators were blinded to the surgical intervention. All experiments were conducted under the UK Home Office Animals (Scientific Procedures) Act 1986, in agreement with local ethical and veterinary approval (Biomedical Research Resources, University of Edinburgh) and the ARRIVE guidelines.

Magnetic Resonance Imaging

Structural T2-weighted, diffusion-tensor (DT), and magnetization transfer (MT) MRI data were collected using a Varian 7T preclinical scanner with a 72 mm volume coil and a four-channel phased array mouse brain coil (see Supplementary Material for detailed methods of image acquisition and protocols). Each T2-weighted MRI slice of the mouse brain was examined from anterior to posterior and recorded for (1) the presence, volume and type of cortical and/or subcortical primary ischemic lesions, classified as hyperintense signal with focal tissue loss, potentially cavitated with or without localized hypointense areas consistent with paramagnetic effects of iron/hemosiderin in the surrounding parenchyma; and (2) primary hemorrhages, their volume and anatomic location, classified as areas of rounded predominantly hypointense signal. Over consecutive T2-weighted MRI slices (1.0 to − 4.6 mm Bregma), the volume of ischemic and hemorrhagic lesions were determined and then combined to give an overall lesion load; brain volume was delineated by measuring the entire volume of the brain covered by MRI (1.0 to − 4.6 mm Bregma) and then data were summed to provide a regional brain volume. Mean diffusivity (MD), fractional anisotropy (FA), and magnetization transfer ratio (MTR) volumes were generated using 'in-house' custom software and the slice corresponding with − 1.2 to − 2.4 mm from the Bregma processed for region of interest analysis.

Assessment of Behavioural Alterations

In 6-month hypoperfused mice, spatial working memory was investigated using an 8-arm radial arm maze; spatial reference learning and memory was investigated using a water maze (see Supplementary Methods).

Pathologic Investigation of Small Vessel Disease

Tissue processing. At the conclusion of the MRI or behavioral assessment, brains were perfusion fixed with paraformaldehyde and paraffin embedded, and coronal sections (6 μm) were cut in agreement with the T2-weighted MRI slices.

Histologic Detection of Ischemic Tissue Damage, Hemorrhage, and Fibrin Accumulation

Sections were stained with hematoxylin and eosin, Perls Prussian blue, and Martius scarlet blue, using standard protocols to determine the presence of ischemic tissue damage, hemorrhage, and vascular accumulation of fibrin. Sections from each anatomic level were screened for the presence and absence of these histologic features.

Immunohistochemical Detection of Myelin, Axonal, Glial, and Vascular Integrity

Adjacent sections to those used for histologic analysis were immunostained using standard methods (see Supplementary Methods). The primary antibodies used were as follows: anti-myelin basic protein (1:300; Millipore, Watford, UK), anti-amyloid precursor protein (1:1,000; Millipore), anti-ionized calcium binding adaptor molecule 1 (Iba1; 1:750; Menarini, Wokingham, UK), anti-fibrinogen (1:5,000; Abcam, Cambridge, UK); anti-glial fibrillary acidic protein (GFAP; 1:100; Life Technologies, Paisley, UK), anti-aquaporin 4 (AQP4; 1:100; Millipore); and collagen IV antibody (1:2,000 (Fitzgerald, MA, USA) or 1:100 (Millipore) for double labeling with GFAP/AQP4). DAPI (4',6-diamidino-2-phenylindole) counterstain was used to identify cell nuclei in some experiments. To assess vascular density, images of the subcortex were acquired (x400) and the percentage of area stained by collagen IV was determined using ImageJ (NIH, Bethesda, MD, USA). Total vessel width was measured in images of the thalamus (x200). Images of GFAP-positive astrocytes and astrocytic endfeet in relation to the vascualture in the thalamus were acquired with a laser scanning confocal microscope (x200; Leica SP5, Leica Microsystems, Milton Keynes, UK). GFAP-positive cell bodies with distinct DAPI-positive nuclei were counted in a grid of defined dimensions. Percentage area stained by AQP4 and collagen IV as well as their respective colocalization (Manders plugin) was determined using NIH ImageJ (Bethesda, MD, USA) software after being equally thresholded across all sections for the respective antibody. The measure of AQP4 outwith vessels was defined as the difference between percentage area stained by AQP4 and collagen IV, respectively.

Quantitation of Claudin-5 Protein

Enzyme-linked Immunosorbent assay (Cusabio) was used to quantify Claudin-5 protein in vessel-enriched fractions (see Supplementary Methods) following the manufacturer's instructions.

Statistical Analysis

For imaging studies, the brain volumes between sham and hypoperfused groups and the brain lesion volume between 1- and 6-month hypoperfused mice were compared using unpaired *t*-tests, with $P < 0.05$. Statistical comparisons of MD, FA, and MTR values between hypoperfused and sham groups were carried out using the Hotelling's Trace multivariate analysis of variance, with follow-up univariate analysis for individual group differences. The percentage of area stained with collagen IV and AQP4, colocalization values, and cell counts were compared between groups using Mann–Whitney U-statistic. Correlative associations were determined using Spearman's correlation coefficient. The frequency distribution of vessel width was compared using the Kolmogorov–Smirnov test. Enzyme-linked Immunosorbent assay data were analyzed using an unpaired *t*-test, with $P < 0.05$. For behavioral studies, the number of novel entries and revisiting errors in the radial arm maze and the path length and escape latency in the water maze were analyzed using a repeated-measures analysis of variance, with trial block as the within-subject factor. Performance in the probe trial of the water maze, measured as the percentage of quadrant occupancy, was compared with chance performance (25%) using a one-sample *t*-test. Differences in the number of

platform crossings and time spent in target zone during the probe test were analyzed using unpaired *t*-tests.

RESULTS

Progression of Radiologic Features and Pathologic Correlates of Small Vessel Disease

All T2-weighted MRI scans were screened for the presence of hyperintense (Figure 1A) and hypointense (Figure 1B) lesions. These radiologic features were confirmed as areas of primary ischemic tissue damage (Figure 1C) and hemorrhagic lesions (Figure 1D) in histologic sections.

Ischemic and Hemorrhagic Lesions

To examine the progression of lesion load and distribution with increasing durations of hypoperfusion, T2-weighted scans were investigated for the presence and anatomic location of primary ischemic and hemorrhagic lesions at 1 ($N=8$ sham; $N=13$ hypoperfused) or 6 months ($N=11$ sham; $N=20$ hypoperfused). Overall, there were no overt lesions present in any of the sham mice. After 1 month of hypoperfusion, the lesion load was minimal: there were no hemorrhagic lesions detected and only 1 mouse from the cohort presented with a small cortical primary ischemic lesion (Figures 2A and 2B). In contrast, a profile of lesions were determined in 6-month hypoperfused mice (Figures 2A and 2B). Primary ischemic lesions were detected in 12 out of the 20 hypoperfused mice. Of these, cortical infarcts, or areas of hyperintensity, were located in the middle cerebral artery territories (see Figure 1A) and found in 9 out of the 20 hypoperfused mice, ranging in volume from 0.04 to 6.2 mm^3. Multiple small focal subcortical infarcts were detected (see Figure 1A) in 7 out of the 20 hypoperfused mice ranging in volume from 0.3 to 3.99 mm^3 (Figure 2B). These were found primarily in the thalamus, but smaller and less frequent lesions were found in the hypothalamus and striatum. Additionally, subcortical cavitated lacunar infarcts were identified in 3 out of the 20 hypoperfused mice as focal regions of hyperintense signal with or without the presence of paramagnetic blood products in the surrounding tissue. Interestingly, the highest lesion load in 6-month hypoperfused mice was related to hemorrhage. In 15 of the 20 hypoperfused mice, hemorrhagic lesions were located in subcortical regions, particularly thalamic nuclei (see Figure 1B), and the lesion load ranged in volume from 0.29 to 15.10 mm^3 (Figure 2B). Overall, in agreement with a progressive pathology, the total lesion load was significantly increased in 6-month compared with 1-month hypoperfused mice ($P<0.05$; Figure 2C).

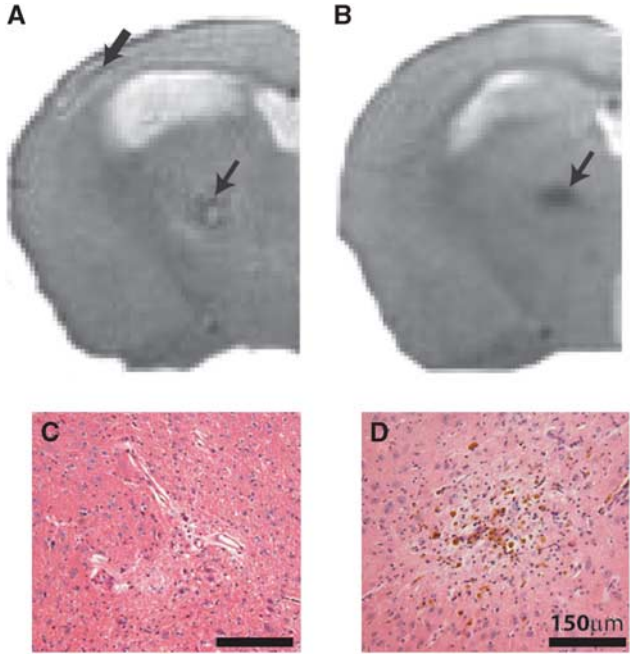

Figure 1. Radiologic features observed on T2-weighted structural magnetic resonance imaging (MRI). Representative images show hyperintense signal in the cortex (**A**; thick arrow) and subcortex (thalamus) (**A**; small arrow), and hypointense signal in the subcortex (**B**; arrow) of 6-month hypoperfused mice (slice taken −1.2 to −2.4 mm from Bregma). Parallel pathologic assessment identified ischemic-like lesions associated with hyperintense features (**C**), and hemorrhagic lesions in the subcortex (**D**) associated with the hypointense signal.

Brain Atrophy

To further explore progressive changes with increasing duration of hypoperfusion, the brain volume was measured on MRI. There was no significant difference in brain volume between sham and hypoperfused mice after 1-month hypoperfusion (Figure 2D; $P>0.05$). However, sustained hypoperfusion for 6 months resulted in a significant decrease in brain volume compared with sham mice (Figure 2D; $P<0.05$). Notably, cerebral atrophy correlated negatively with total lesion load ($r=-0.5636$, $P<0.01$).

White Matter Disruption

Previously, we identified white matter disruption after 1 month of hypoperfusion[21] and aimed to determine the impact of 6 months of hypoperfusion on white matter integrity using MRI. We had shown previously that white matter changes primarily occur in the corpus collosum at the slice corresponding with −1.2 to −2.4 mm from Bregma. Table 1 provides a summary of white matter disruption and subcortical alterations in 6-month hypoperfused mice ($N=20$) compared with sham mice ($N=11$) as assessed by DT- and MT-MRI biomarkers. The Hotelling's Trace multivariate test of overall differences among groups was statistically significant for the corpus callosum ($P<0.005$), internal capsule ($P<0.004$), fimbria ($P<0.004$), and subcortex ($P<0.04$). Follow-up univariate *post hoc* comparisons (Table 1) showed that FA was significantly reduced in the corpus callosum, internal capsule, and fimbria, but was significantly increased in the subcortex. MTR was minimally altered between groups, and reductions in MTR were only significant in the fimbria, the tract demonstrating the highest level of disruption with FA. MD was not significantly altered in any region studied. Immunohistochemical staining revealed a disruption of myelinated fibers, and evidence of axonal pathology in the hypoperfused mice in white matter tracts including the corpus callosum, internal capsule, and fimbria associated with increased microglia (Supplementary Figure 1).

Gliovascular Alterations

Collagen IV immunostaining was used to determine whether changes in vascular basement membrane structure may occur subcortically in response to hypoperfusion at 1 month ($N=6$ sham; $N=14$ hypoperfused) and 6 months ($N=14$ sham; $N=15$ hypoperfused). After 1 month hypoperfusion, there was no significant change in the density of collagen IV staining (Figures 3A and 3B; $U=28.0$, $P>0.05$). However, at 6 months of hypoperfusion, there was a significant increase in the density of collagen IV staining (Figures 3A and 3B; $U=54.0$, $P<0.05$). The widths of longitudinal vessels were further measured in the subcortex of hypoperfused and sham mice. There was no change in vessel width after 1 month of hypoperfusion (Figure 3C; $D=0.0613$, $P>0.05$). Conversely, after 6 months of hypoperfusion, there was a significant increase in total vessel width (Figure 3C;

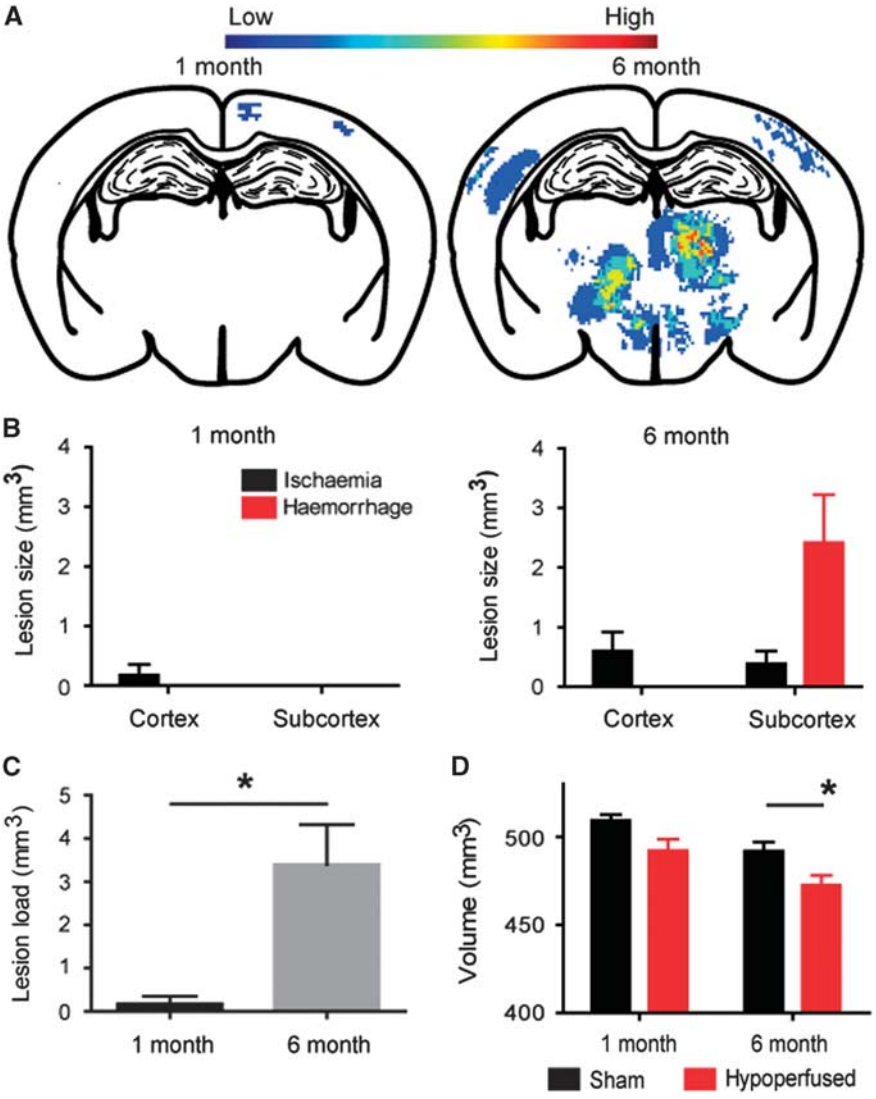

Figure 2. Progression of pathology in response to cerebral hypoperfusion. Heat maps depicting lesion load in the hypoperfused mice after 1 ($N=8$ sham; $N=13$ hypoperfused) and 6 ($N=11$ sham; $N=20$ hypoperfused) months (**A**) are indicated by color ranging from low to high occurrence. This brain slice is shown as it contained the highest lesion load in the thalamus and cortex at 6 months after hypoperfusion. After 1 month of hypoperfusion, lesion load throughout the brain is minimal, exclusively ischemic and confined to the cortex (**B**). With increased duration of hypoperfusion to 6 months, cortical and subcortical lesions are evident throughout the brain (**B**). Subcortical hemorrhages represented the major lesion burden with a smaller load of cortical and subcortical ischemic lesions (**B**). Overall, there was significantly greater total lesion load in the 6-month compared with 1-month hypoperfused mice (**C**). Additionally, there was a significant decrease in total brain volume in 6-month hypoperfused mice, whereas the brain volume was not changed in the 1-month cohort (**D**). *$P<0.05$.

$D=0.170$, $P<0.001$) when compared with age-matched sham animals.

Further investigation of the underlying mechanisms associated with the vascular pathology in 6-month hypoperfused mice was undertaken with a range of histologic markers (hematoxylin and eosin, Martius scarlet blue, Perls; Figure 3D). Notably, this revealed the presence of fibrin within the vascular wall, in subcortical areas, of 12 out of the 20 hypoperfused mice. The presence of hemosiderin-laden macrophages surrounding the vascular lesions (Figure 3D) was identified in all of the mice with evidence of fibrinoid necrosis. There was also positive Perl's staining present in an additional four hypoperfused mice. Fibrinogen accumulation within the parenchyma was also observed supportive of BBB breakdown (Figure 3D). A pronounced microglial response surrounding the vascular lesions was also detected (Figure 3D).

To further investigate whether the BBB may be progressively disrupted in the model, the levels of Claudin-5, a component of tight junctions within the BBB, were determined by enzyme-linked immunosorbent assay at 1 month ($N=8$ sham; $N=6$ hypoperfused; Figure 3E) and 6 months ($N=10$ sham; $N=9$ hypoperfused; Figure 3F). Although there were no significant changes in the levels of Claudin-5 after 1 month of hypoperfusion, the levels were significantly decreased after 6 months in the hypoperfused when compared with age-matched sham animals ($P<0.05$).

As there is a close relationship between the vasculature, BBB, and astrocytes, we hypothesized that these prominent vascular changes would be associated with astrocytic changes. GFAP-positive astrocytes were counted within the thalamus after 1 month ($N=8$ sham, $N=13$ hypoperfused) and 6 months ($N=11$ sham, $N=20$ hypoperfused). After 1 month of hypoperfusion, there was no significant difference in astrocyte numbers (Figures

Table 1. Diffusion tensor and magnetization transfer MRI biomarker values in long-term hypoperfused ($N = 20$) and sham ($N = 11$) mice

Region of interest	*Biomarker*	*Sham*	*Hypoperfused*	*Statistics*	*% Change*
Corpus callosum	FA	0.45 ± 0.01	0.41 ± 0.01	$F_{(1,25)} = 13.9$, $P = 0.001$	−8.33
	MTR	29.7 ± 0.68	29.2 ± 0.38	$F_{(1,25)} = 0.45$, $P = 0.508$	−1.65
	MD	6.58 ± 0.14	6.91 ± 0.12	$F_{(1,25)} = 3.00$, $P = 0.096$	+4.88
Internal capsule	FA	0.50 ± 0.01	0.37 ± 0.02	$F_{(1,25)} = 21.9$, $P = 0.000$	−33.0
	MTR	30.2 ± 1.00	30.0 ± 0.42	$F_{(1,25)} = 0.36$, $P = 0.792$	−0.82
	MD	7.15 ± 0.29	7.23 ± 0.25	$F_{(1,25)} = 0.00$, $P = 0.956$	+1.23
Fimbria	FA	0.56 ± 0.02	0.42 ± 0.03	$F_{(1,25)} = 10.5$, $P = 0.004$	−35.5
	MTR	29.1 ± 0.64	24.7 ± 1.40	$F_{(1,25)} = 14.4$, $P = 0.001$	−17.9
	MD	9.14 ± 0.22	10.6 ± 0.02	$F_{(1,25)} = 2.39$, $P = 0.136$	+4.00
Subcortex	FA	0.26 ± 0.01	0.28 ± 0.01	$F_{(1,25)} = 8.34$, $P = 0.008$	+7.14
	MTR	27.2 ± 0.61	27.9 ± 0.39	$F_{(1,25)} = 1.04$, $P = 0.317$	+2.26
	MD	7.23 ± 0.12	7.30 ± 0.09	$F_{(1,25)} = 0.03$, $P = 0.866$	−0.95

Abbreviations: FA, fractional anisotropy; MD, mean diffusivity; MRI, magnetic resonance imaging; MTR, magnetization transfer ratio. Cerebral hypoperfusion (6 months) results in significant reductions in FA in the corpus callosum, internal capsule, and fimbria, along with a significant atypical increase in the subcortex, suggesting underlying axonal disruption. MTR (%) is significantly reduced in the fimbria only, whereas MD ($\times 10^{-4}$ mm^2/s) is not significantly altered in any of the regions studied.

4A and 4B), but at 6 months there was a significant increase in the number of GFAP-positive astrocytes observed in comparison with sham animals (Figures 4A and 4C; $U = 39.0$, $P < 0.01$).

To better understand potential dynamic changes in the gliovasculature, alterations in the astrocytic endfoot protein AQP4 was investigated. The mean percentage area (± s.e.m.) covered by AQP4 was not significantly different between shams or hypoperfused mice, respectively, after either 1 month (15.2 ± 4.3 versus 15.2 ± 2.8) or 6 months (8.4 ± 2.9 versus 20.3 ± 5.3) of hypoperfusion, although a trend toward an increase at 6 months was observed ($U = 72$, $P = 0.12$). Similarly, after 1 month and 6 months, the percentage of AQP4 colocalized to collagen IV-positive vessels as well as AQP4 found within the parenchyma was not significantly different, although after 6 months, there was a decrease in the amount of AQP4 colocalized to vessels and an increase in the amount of AQP4 located within the parenchyma (AQP4 outwith vessels), suggestive of redistribution of the water channel (Figure 5). In support of this, the levels of AQP4 outwith vessels within the parenchyma was negatively correlated to vascular AQP4 (Figure 6F; $r = -0.7429$, $P < 0.001$).

Cognitive Assessment

Impairment of spatial working memory. In humans, SVD is often associated with impaired working memory, and thus we sought to determine whether spatial working memory, as measured using the radial arm maze, would be impaired in the mouse model with features of SVD ($N = 14$ sham; $N = 14$ hypoperfused). In support of this, a robust impairment in working memory performance was seen in the hypoperfused group (Figure 6A), with the number of novel arm entries made in the first 8-arm choices being significantly lower ($F_{(1,\ 26)} = 18.0$, $P < 0.001$) and the number of revisiting errors being significantly higher ($F_{(1,26)} = 12.9$, $P < 0.002$) compared with the sham mice. There was a significant improvement in learning across days by both groups, with the number of new arms visited increasing ($F_{(7,182)} = 10.88$, $P < 0.001$) and the number of errors committed decreasing significantly over the training period ($F_{(4.2,111.1)} = 17.03$, $P < 0.001$).

Impairment of spatial reference learning and memory. Previously, we demonstrated that 1 month of hypoperfusion does not influence spatial reference learning and memory at a time when there are deficits in working memory and subtle white matter alterations;[20] however with increasing duration of hypoperfusion and degenerative processes, we hypothesized this may result in a progressive impairment in cognitive abilities. Initial training on a cue task showed that sensorimotor function and basic learning was not impaired by hypoperfusion (data not shown). After the cue task, the mice underwent 7 days of hidden platform training in the water maze (Figure 6B). Spatial learning was impaired in the hypoperfused mice; escape latency ($F_{(1,26)} = 12.0$, $P < 0.005$) and path length ($F_{(1,27)} = 8.51$, $P < 0.01$) were significantly increased compared with sham mice. Both groups of mice were able to learn the platform location with a significant reduction in escape latency ($F_{(6,156)} = 12.4$, $P < 0.001$) and path length ($F_{(6,156)} = 14.4$, $P < 0.001$) over the training days. To assess long-term spatial reference memory, two probe tests were conducted. In the first probe test conducted on the last day of the 7-day training trial (Figures 6C and 6D), the time spent in the training quadrant was significantly above chance in the sham group ($P < 0.005$) but not the hypoperfused group ($P > 0.05$). Moreover, the hypoperfused mice conducted significantly fewer platform crossings ($F_{(1,26)} = 9.1$, $P < 0.01$) and also spent significantly less time in the target area ($F_{(1,\ 26)} = 5.5$, $P < 0.05$) than sham mice. Similarly, hypoperfused mice were impaired as compared with shams in the second probe test conducted 24 hours after the last training trial (data not shown).

DISCUSSION

Despite the increasing burden of SVD, progress towards understanding the pathophysiology and development of treatment strategies has been hampered, in part, because of the lack of relevant animal models. Here, we have evaluated a mouse model,[19,20] which recapitulated some radiologic and pathologic features of SVD as well as impairment in spatial working and reference memory. Investigation of the associated pathologic correlates indicated prominent disruption of the gliovasculature including BBB breakdown.

To date, several animal models have been developed, which mimic various pathologic features of SVD.[11,12] Rodent models of hypoperfusion have mainly been studied to provide mechanistic insight into the pathophysiology of white matter lesions, which are a manifestation of SVD. Previously, we demonstrated that a short, 1-month period of cerebral hypoperfusion causes subtle alterations in white matter integrity as determined by

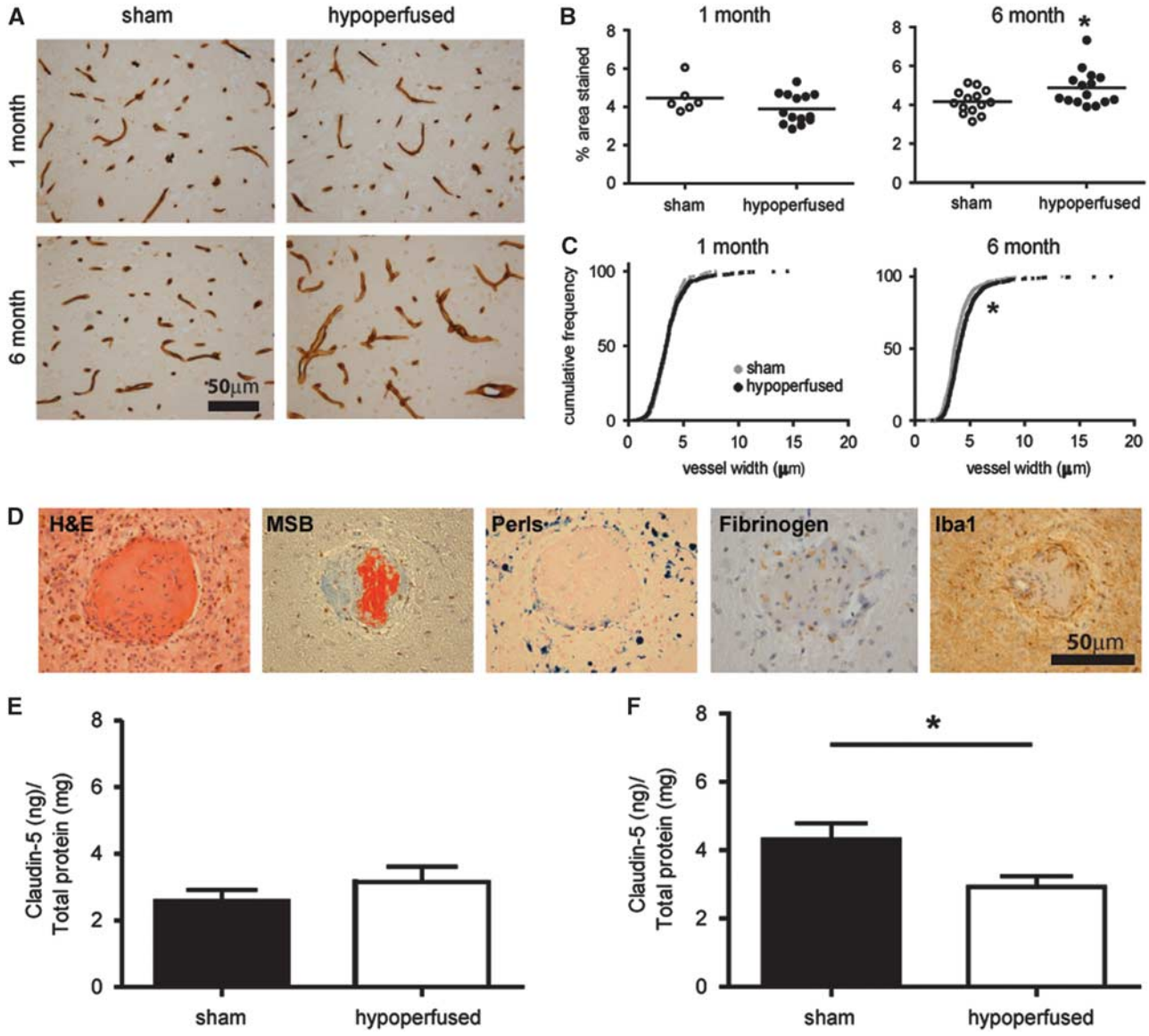

Figure 3. Pronounced vascular alterations and blood–brain barrier (BBB) breakdown. Collagen IV staining in sham and hypoperfused mice after 1 month ($N=$ 6 sham; $N=14$ hypoperfused) or 6 months ($N=14$ sham; $N=15$ hypoperfused)(**A**). One-month hypoperfusion had no significant effect on density (**B**) or vessel width (**C**) in the subcortex (thalamus). In comparison, 6 months of hypoperfusion resulted in a significant increase in collagen IV density (**A**) and vessel width (**B**) within the thalamus. Evidence of fibrinoid necrosis is observed in hypoperfused mice (in 12 out of the 20) with vascular disruption (**D**) observed on hematoxylin and eosin (H&E) and Martius scarlet blue (MSB), with collagen accumulation, vessel wall enlargement, and fibrin deposition (red in MSB); surrounding hemosiderin blood products (Perls), parenchymal fibrogen accumulation, and inflammatory cells (ionized calcium binding adaptor molecule 1, Iba1) suggest BBB disruption and macrophage activation (features absent in 6-month sham mice, $N=11$). Quantification of Claudin-5 in vessel-enriched fractions by enzyme-linked Immunosorbent assay (ELISA) showed no changes in the levels of the protein after 1 month (**E**; $N=8$ sham; $N=6$ hypoperfused); in contrast, a significant decrease was found after 6 months in the hypoperfused group when compared with sham mice (**F**; $N=10$ sham; $N=9$ hypoperfused). $^*P<0.05$.

immunohistochemical approaches[20,22] and DT-MRI.[21] The present study illustrates that with sustained carotid stenosis, over 6 months, there is a progressive deterioration in white matter integrity. The radiologic findings are similar to those previously reported by our group, whereby FA and MTR are altered after short-term hypoperfusion. In the present study, which examines a longer period of carotid stenosis, the magnitude of the FA/MTR changes are more pronounced, which is in agreement with our findings of significantly increased radiologic features of SVD and reduced brain volume after prolonged hypoperfusion. Consistent with our previously published data,[21] there was no change in MD detected in our model, which is somewhat unexpected as MD is a marker of white matter damage in SVD in humans.[27] A recent study has also shown that other DTI measures (AD and RD) may be sensitive to the effects of cerebral hypoperfusion, and for future studies, these additional measures would be advisable to study.[28] Notably, in the same animals in which imaging was conducted, we observed myelin and axonal disruption alongside a prominent inflammatory response.

In addition to white matter pathology, sustained hypoperfusion leads to widespread vascular disruption and progressive cognitive decline. In particular, there is a marked increase in vessel width and collagen IV density, fibrinoid necrosis, and hemorrhage, features that are all absent from short-term hypoperfused or age-

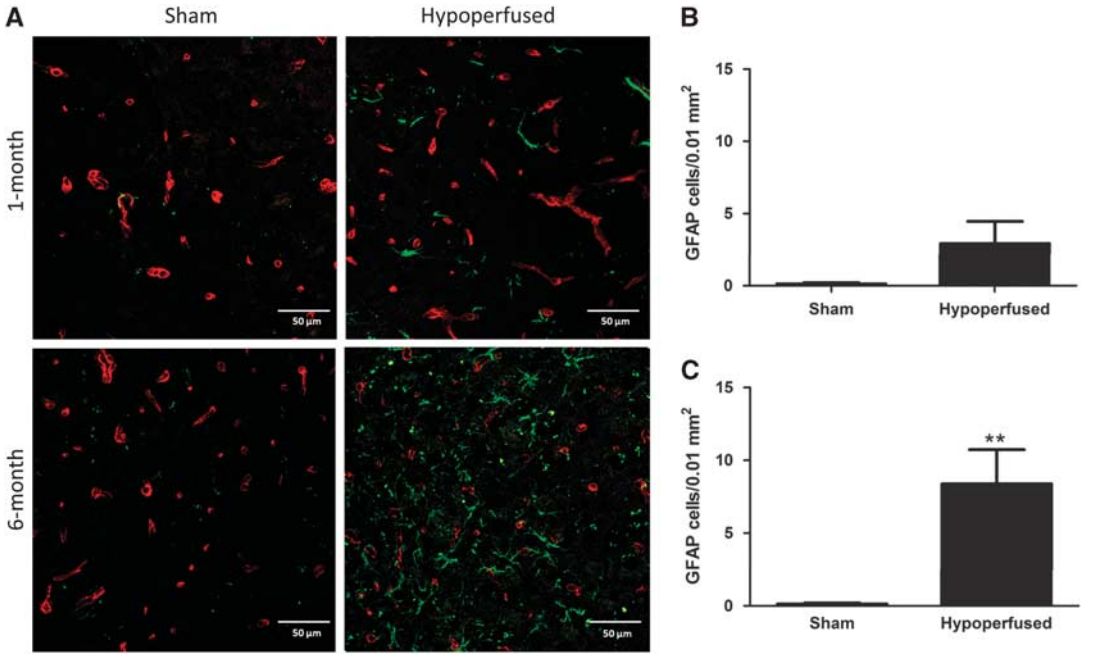

Figure 4. Increased astrocyte number after long-term hypoperfusion. Representative images of glial fibrillary acidic protein (GFAP) (green) and collagen IV (red) double immunostaining in the thalamus of sham and hypoperfused mice after 1 month ($N = 8$ sham; $N = 13$ hypoperfused) and 6 months ($N = 11$ sham; $N = 20$ hypoperfused) (**A**). One month of hypoperfusion had no significant effect on astrocyte number (**B**), whereas at 6 months there was a significant increase in comparison with shams (**C**). $^{**}P < 0.01$.

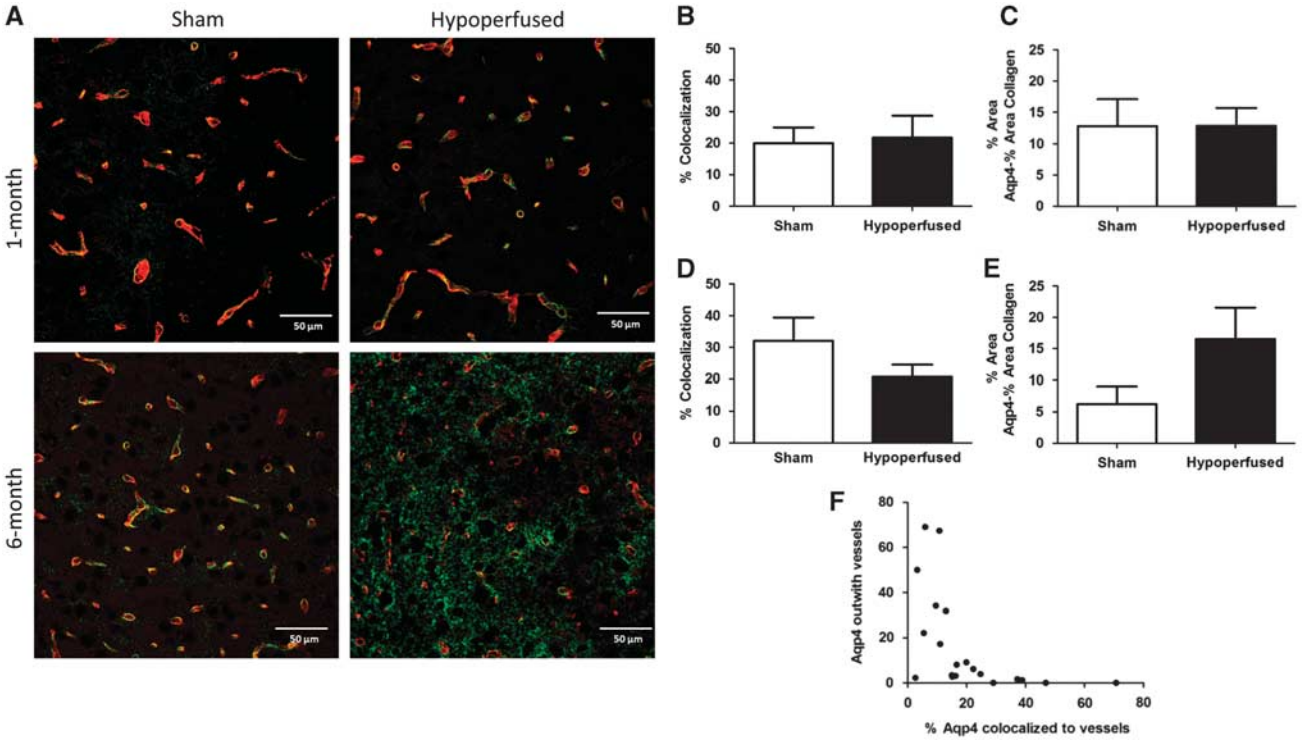

Figure 5. Displacement of aquaporin 4 (AQP4) after long-term hypoperfusion. Representative images of AQP4 (green) and collagen IV (red) double immunostaining staining in the thalamus of sham and hypoperfused mice after 1 month ($N = 8$ sham; $N = 13$ hypoperfused) and 6 months ($N = 11$ sham; $N = 20$ hypoperfused) (**A**). One month of hypoperfusion had no significant effect on the percentage of AQP4 colocalized to vessels or to the parenchymal AQP4 levels ouwith the vessels (**B** and **C**); however, at 6 months there was evidence of a redistribution of AQP4, with a trend toward both a decrease in AQP4 colocalizing to vessels and an increase in parenchymal AQP4 outwith the vasculature (**D** and **E**). The percentage of vascular-associated AQP4 was negatively correlated ($P < 0.001$) with parenchymal AQP4 levels (**F**).

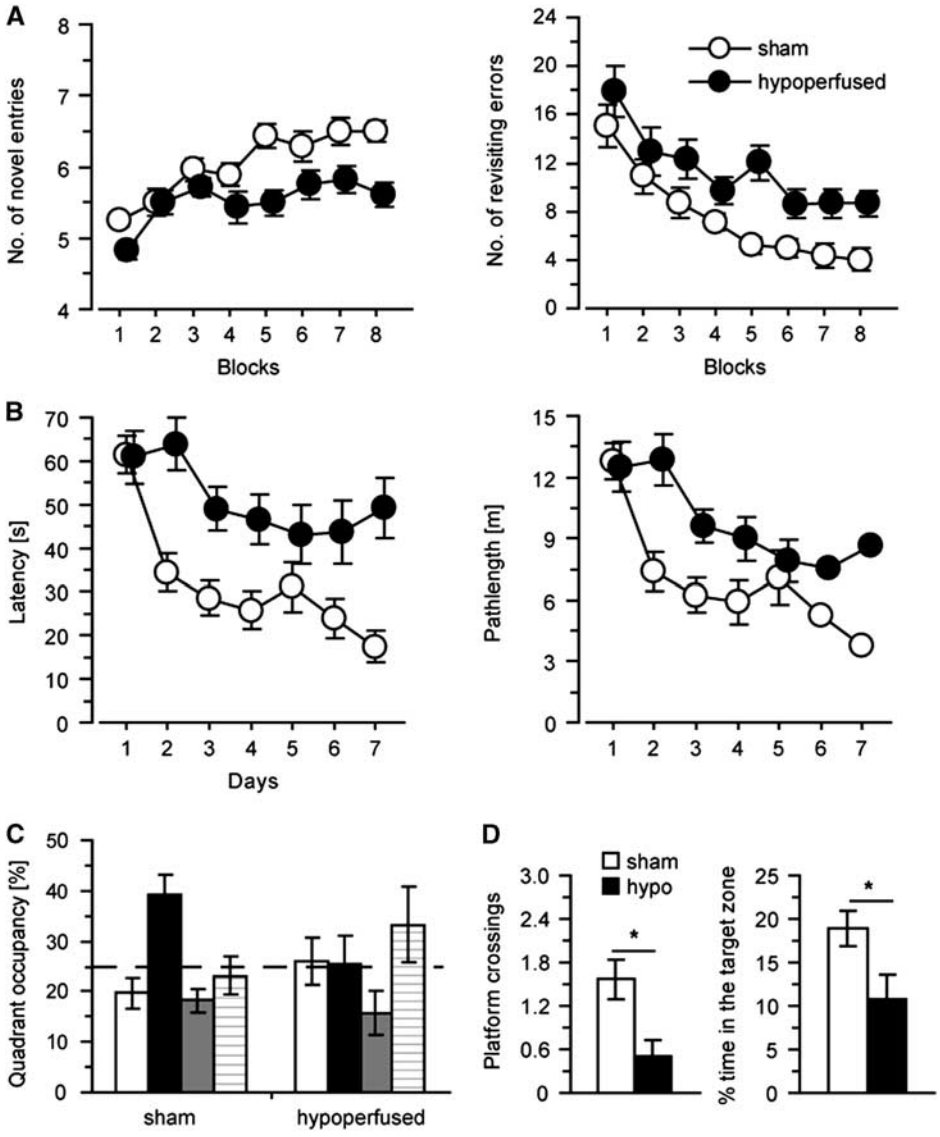

Figure 6. Cognitive impairments after long-term hypoperfusion ($N = 14$ per group). Spatial working memory was impaired in hypoperfused mice, performing significantly less novel arm entries and significantly greater revisiting errors (**A**). Analysis of spatial reference learning and memory in the water maze identified a significant deficit in latency and path length (**B**) in the hidden platform task. Data are shown from the first probe trial to examine long-term spatial reference memory (**C** and **D**). Sham mice showed better-than-chance performance when compared with hypoperfused mice who did not reach chance performance. Hypoperfused mice also conducted significantly less platform crossings (**D**) and spent less time (**D**) in the target area than sham mice. $^*P < 0.05$.

matched controls. Disrupted penetrating arteries and arterioles are common in SVD, often characterized as lipohyalinosis with or without evidence of fibrinoid necrosis. The demonstration of vascular-related features, which are similar to human SVD,[29] including vessel wall disruption, collagen IV accumulation, fibrin deposition, and cavitated lacunar-type infarcts, highlights the relevance of this mouse model as a tool to explore underlying mechanisms of vascular disease. Such focal vascular disruptions were often associated with hemosiderin-laden macrophages, consistent with microbleeds. The presence of overt vascular disruption and BBB breakdown in our model is in agreement with clinical observations, suggesting that BBB disruption is a key mechanism involved in pathogenesis of human SVD.[9] To investigate the role of vascular integrity in disease progression, we measured collagen IV density and vessel width after acute and long-term hypoperfusion. Interestingly, the density of collagen IV staining, as a marker of basement membranes, was not altered after 1-month hypoperfusion, but was significantly increased at the longer time point. To further examine the progression of BBB disruption with increasing hypoperfusion, the levels of claudin-5, a transmembrane protein present at the tight junctions, was determined. Notably, 1 month of hypoperfusion had no effect in the levels of the protein, but a significant decrease was found after 6 months. Fibrinogen accumulation wihin the parenchyma was also noted at 6 months of hypoperfusion, supportive of BBB breakdown. Vascular-related changes were predominantly observed in subcortical regions, particularly the thalamus, and also in the caudate with long-term carotid stenosis. Recently, it has been shown that chronic cerebral hypoperfusion leads to vascular wall remodeling.[28] These changes may potentially lead to sheer stress in the vessels in the anterior and posterior circulation, subsequent endothelial alterations, and BBB breakdown.

Coincident with cerebrovascular changes, long-term hypoperfusion also led to marked alterations in glia. We found an increase in

GFAP-positive astrocytes within the thalamus of 6-month hypoperfused mice, indicative of reactive gliosis, which is commonly observed in the brains of individuals with SVD.[8] Reactive astrocytosis was accompanied by a mislocalization of AQP4 from the vasculature to the parenchyma. AQP4 is a water channel typically confined to the astrocytic endfeet of vascular-associated astrocytes, and although the physiologic role of AQP4 is not clear, it is reported to maintain osmotic balance. Loss of AQP4 polarization to the perivascular endfeet has been reported to occur after ischemic events including the development of microinfarcts.[30,31] AQP4 may act to remove edema after injury,[30] but this change in polarity can also be accompanied by disruption of the BBB.[32] In the present study, BBB alterations were coincident with reactive astrocytosis and AQP4 polarization. Whether these changes are causative of BBB disruption or a direct reaction is not entirely clear. The precise mechanism leading to these gliovascular alterations remains to be identified. Our previous work showed that early in response to hypoperfusion there is activation of inflammatory and angiogenic pathways coincident with disruption of axon–glial integrity.[22] Others have reported an involvement of the renin–angiotensin system[28,33] and oxidative stress pathways.[28] It should also be noted that the microcoils themselves may cause an additional inflammatory stimuli contributing to the degenerative changes. Overall, the present study adds to these studies and highlights the detrimental effects of longer-term hypoperfusion on gliovascular alterations, identifying a potential mechanism of disruption in this model, which may allow targeted intervention studies.

In addition, sustained hypoperfusion resulted in significant impairments both in spatial working memory and in acquisition and memory deficits in a spatial reference memory task. Previously, we reported, after 1 month of hypoperfusion, that working memory was impaired while reference memory remained intact, and suggested that this was a result of the disruption of the frontal cortical circuitry.[20] The emergence of deficits in both working and reference memory with long-term hypoperfusion likely reflects the presence of white and gray matter pathology including brain atrophy. These findings are in agreement with a previous study, which examined the effects of long-term hypoperfusion using a battery of behavioral tasks and similarly reported spatial reference and working memory impairments.[24] This study of Nishio *et al*,[24] whilst focusing on behavioral alterations that occur long term in the hypoperfusion model, also reported metabolic alterations using 18F-fluorodeoxyglucose positron emission tomography and hippocampal atrophy, but did not report the subcortical pathologic features (microinfarcts/microbleeds). The results from the present study additionally highlight a spectrum of pathologic alterations coincident with a pronounced cognitive impairment and indicate that longer-term hypoperfusion more accurately replicates features of SVD in humans.

A major strength of the current study is the demonstration of ultrastructural alterations in white matter and subcortical nuclei using quantitative MRI biomarkers. Human data have indicated that such measures may more accurately model disease burden and reflect degree of cognitive decline compared with overt radiologic features.[34] In agreement with this, we observed multiple subtle pathologic alterations in hypoperfused mice, which individually were not sufficient to be visible on T2-weighted MRI screening, although global brain atrophy was very evident, suggesting that while critical for SVD diagnosis, especially in humans where acute pathologic confirmation is often impossible, the need for more advanced imaging methods is required to detect the full spectrum of disease presentation.

As yet, the mechanisms causing predisposition to SVD are not known. Vascular risk factors including diabetes and hypertension were reported to have a key role in the epidemiology of SVD, with hypertension thought to be the most important modifiable risk factor. However, it has since been shown that all vascular risk factors combined account for $<2\%$ of the variance in white matter hyperintensities.[2] Furthermore, despite major advances in blood pressure control, the incidence of SVD remains high, and this has failed to prevent the progression of white matter hyperintensities or lacunar stroke,[35] suggesting that other risk factors may be crucial to disease progression. Recent evidence from animal models also suggest that hypertension is not the key driver of white matter changes.[36,37] Our results show that some radiologic, pathologic, and cognitive features of human SVD can be recapitulated in a mouse model by common carotid stenosis. Our findings also provide evidence that hypoperfusion may precipitate SVD-like disease culminating in a progressive brain and gliovascular pathology. The model may provide opportunities for testing novel treatment strategies for this highly prevalent disabling condition.

DISCLOSURE/CONFLICT OF INTEREST

The authors have no conflict of interest to declare.

ACKNOWLEDGMENTS

The authors thank Dr Jansen, Gray, and MacGillivray for their support with imaging and processing.

REFERENCES

1 van Dijk EJ, Prins ND, Vrooman HA, Hofman A, Koudstaal PJ, Breteler MM. Progression of cerebral small vessel disease in relation to risk factors and cognitive consequences: Rotterdam Scan Study. *Stroke* 2008; **39**: 2712–2719.
2 Wardlaw JM, Allerhand M, Doubal FN, Valdes Hernandez M, Morris Z, Gow AJ *et al.* Vascular risk factors, large-artery atheroma, and brain white matter hyperintensities. *Neurology* 2014; **82**: 1331–1338.
3 Kalaria RN. Cerebrovascular disease and mechanisms of cognitive impairment: evidence from clinicopathological studies in humans. *Stroke* 2012; **43**: 2526–2534.
4 Pantoni L. Cerebral small vessel disease: from pathogenesis and clinical characteristics to therapeutic challenges. *Lancet Neurol* 2010; **9**: 689–701.
5 Fernando MS, Ince PG. Vascular pathologies and cognition in a population-based cohort of elderly people. *J Neurol Sci* 2004; **226**: 13–17.
6 Roman GC, Erkinjuntti T, Wallin A, Pantoni L, Chui HC. Subcortical ischaemic vascular dementia. *Lancet Neurol* 2002; **1**: 426–436.
7 Dichgans M, Holtmannspotter M, Herzog J, Peters N, Bergmann M, Yousry TA. Cerebral microbleeds in cadasil: a gradient-echo magnetic resonance imaging and autopsy study. *Stroke* 2002; **33**: 67–71.
8 Gouw AA, Seewann A, van der Flier WM, Barkhof F, Rozemuller AM, Scheltens P *et al.* Heterogeneity of small vessel disease: a systematic review of mri and histopathology correlations. *J Neurol Neurosurg Psychiatry* 2011; **82**: 126–135.
9 Wardlaw JM, Smith C, Dichgans M. Mechanisms of sporadic cerebral small vessel disease: insights from neuroimaging. *Lancet Neurol* 2013; **12**: 483–497.
10 Abbott NJ, Rönnbäck L, Hansson E. Astrocyte–endothelial interactions at the blood–brain barrier. *Nat Rev Neurosci* 2006; **7**: 41–53.
11 Hachinski V, Iadecola C, Petersen RC, Breteler MM, Nyenhuis DL, Black SE *et al.* National Institute of Neurological Disorders and Stroke-Canadian Stroke Network vascular cognitive impairment harmonization standards. *Stroke* 2006; **37**: 2220–2241.
12 Bailey EL, McCulloch J, Sudlow C, Wardlaw JM. Potential animal models of lacunar stroke: a systematic review. *Stroke* 2009; **40**: e451–e458.
13 Hainsworth AH, Markus HS. Do *in vivo* experimental models reflect human cerebral small vessel disease? A systematic review. *J Cereb Blood Flow Metab* 2008; **28**: 1877–1891.
14 Bailey EL, Wardlaw JM, Graham D, Dominiczak AF, Sudlow CL, Smith C. Cerebral small vessel endothelial structural changes predate hypertension in stroke-prone spontaneously hypertensive rats: a blinded, controlled immunohistochemical study of 5- to 21-week-old rats. *Neuropathol Appl Neurobiol* 2011; **37**: 711–726.
15 Tagami M, Nara Y, Kubota A, Sunaga T, Maezawa H, Fujino H *et al.* Ultrastructural characteristics of occluded perforating arteries in stroke-prone spontaneously hypertensive rats. *Stroke* 1987; **18**: 733–740.
16 Niklass S, Stoyanov S, Garz C, Bueche CZ, Mencl S, Reymann K *et al.* Intravital imaging in spontaneously hypertensive stroke-prone rats—a pilot study. *Exp Transl Stroke Med* 2014; **6**: 1.

17 Braun H, Bueche CZ, Garz C, Oldag A, Heinze HJ, Goertler M *et al.* Stases are associated with blood–brain barrier damage and a restricted activation of coagulation in SHRSP. *J Neurol Sci* 2012; **322**: 71–76.
18 Tagami M, Nara Y, Kubota A, Fujino H, Yamori Y. Ultrastructural changes in cerebral pericytes and astrocytes of stroke-prone spontaneously hypertensive rats. *Stroke* 1990; **21**: 1064–1071.
19 Shibata M, Ohtani R, Ihara M, Tomimoto H. White matter lesions and glial activation in a novel mouse model of chronic cerebral hypoperfusion. *Stroke* 2004; **35**: 2598–2603.
20 Coltman R, Spain A, Tsenkina Y, Fowler JH, Smith J, Scullion G *et al.* Selective white matter pathology induces a specific impairment in spatial working memory. *Neurobiol Aging* 2011; **32**: 2324 e2327–e2312.
21 Holland PR, Bastin ME, Jansen MA, Merrifield GD, Coltman RB, Scott F *et al.* MRI is a sensitive marker of subtle white matter pathology in hypoperfused mice. *Neurobiol Aging* 2011; **32**: 2325 e2321–e2326.
22 Reimer MM, McQueen J, Searcy L, Scullion G, Zonta B, Desmazieres A *et al.* Rapid disruption of axon–glial integrity in response to mild cerebral hypoperfusion. *J Neurosci* 2011; **31**: 18185–18194.
23 Farkas E, Donka G, de Vos RA, Mihaly A, Bari F, Luiten PG. Experimental cerebral hypoperfusion induces white matter injury and microglial activation in the rat brain. *Acta Neuropathol* 2004; **108**: 57–64.
24 Nishio K, Ihara M, Yamasaki N, Kalaria RN, Maki T, Fujita Y *et al.* A mouse model characterizing features of vascular dementia with hippocampal atrophy. *Stroke* 2010; **41**: 1278–1284.
25 Potter GM, Doubal FN, Jackson CA, Sudlow CL, Dennis MS, Wardlaw JM. Lack of association of white matter lesions with ipsilateral carotid artery stenosis. *Cerebrovasc Dis* 2012; **33**: 378–384.
26 Fernando MS, Simpson JE, Matthews F, Brayne C, Lewis CE, Barber R *et al.* White matter lesions in an unselected cohort of the elderly: molecular pathology suggests origin from chronic hypoperfusion injury. *Stroke* 2006; **37**: 1391–1398.
27 Muñoz Maniega S, Valdés Hernández M, Clayden JD, Royle NA, Murray C, Morris Z *et al.* White matter hyperintensities and normal-appearing white matter integrity in the ageing brain. *Neurobiol Aging* 2015; doi: 10.1016/j.neurobiolaging.2014.07.048.
28 Füchtemeier M, Brinckmann MP, Foddis M, Kunz A, Po C, Curato C *et al.* Vascular change and opposing effects of the angiotensin type 2 receptor in a mouse model of vascular cognitive impairment. *J Cereb Blood Flow Metab* 2014; doi:10.1038/jcbfm.2014.221.
29 Craggs LJ, Yamamoto Y, Deramecourt V, Kalaria RN. Microvascular pathology and morphometrics of sporadic and hereditary small vessel diseases of the brain. *Brain Pathol* 2014; **24**: 495–509.
30 Wang M, Iliff JJ, Liao Y, Chen MJ, Shinseki MS, Venkataraman A *et al.* Cognitive deficits and delayed neuronal loss in a mouse model of multiple microinfarcts. *J Neurosci* 2012; **32**: 17948–17960.
31 Steiner E, Enzmann GU, Lin S, Ghavampour S, Hannocks MJ, Zuber B *et al.* Loss of astrocyte polarization upon transient focal brain ischemia as a possible mechanism to counteract early edema formation. *Glia* 2012; **60**: 1646–1659.
32 Wolburg-Buchholz K, Mack AF, Steiner E, Pfeiffer F, Engelhardt B, Wolburg H. Loss of astrocyte polarity marks blood–brain barrier impairment during experimentalautoimmune encephalomyelitis. *Acta Neuropathol* 2009; **118**: 219–233.
33 Dong YF, Kataoka K, Toyama K, Sueta D, Koibuchi N, Yamamoto E *et al.* Attenuation of brain damage and cognitive impairment by direct renin inhibition in mice with chronic cerebral hypoperfusion. *Hypertension* 2011; **58**: 635–642.
34 van Norden AG, de Laat KF, van Dijk EJ, van Uden IW, van Oudheusden LJ, Gons RA *et al.* Diffusion tensor imaging and cognition in cerebral small vessel disease the RUN DMC study. *Biochim Biophys Acta* 2012; **1822**: 401–407.
35 SPS3 Study Group, Benavente OR, Coffey CS, Conwit R, Hart RG, McClure LA *et al.* Blood-pressure targets in patients with recent lacunar stroke: the SPS3 randomised trial. *Lancet* 2013; **382**: 507–515.
36 Holland PR, Pannozzo MA, Bastin M, McNeilly AD, Ferguson KJ, Caughey S *et al.* Hypertension fails to disrupt white matter integrity in young or aged Fisher (F44) Cyp1a1Ren2 transgenic rats. *J Cereb Blood Flow Metab* 2015; **35**: 188–92.
37 Brittain JF, McCabe C, Khatun H, Kaushal N, Bridges LR, Holmes WM *et al.* An MRI-histological study of white matter in stroke-free SHRSP. *J Cereb Blood Flow Metab* 2013; **33**: 760–763.

Supplementary Information accompanies the paper on the Journal of Cerebral Blood Flow & Metabolism website (http://www.nature.com/jcbfm)